relationships obtained under normal conditions to the 3-parameter logarithmic functions (*Eq. 1 and 2*) using the least square method. We averaged the F and H values of the left and the right heart for the 7 animals. The averaged values were used as the standard F and H parameters in subsequent analyses.

Estimation of the integrated cardiac output curve Using the standard F and H parameters, we examined whether we could estimate the integrated cardiac output curve from a single set of CO, P_{LA} and P_{RA} values. For each animal in *Group 1*, we calculated the S parameter by substituting the reference values of CO, P_{LA} and P_{RA} into *Eq. 1* and *2*. This calculation was done under normal and heart failure conditions. After calculating the S parameter, the P_{LA} and P_{RA} measured in each step were substituted into *Eq. 1* to estimate CO of the left heart and into *Eq. 2* to estimate CO of the right heart, respectively. The estimated and measured CO were compared by linear regression analyses.

Prediction of circulatory equilibrium In the other 8 dogs (*Group 2*), we estimated both the integrated cardiac output curve and venous return surface. The cardiac output curve was estimated as described above, using the standard F and H parameters. Venous return surface was estimated according to our previous work (29) using the following formula.

$$CO_V = V/0.129 - 19.61P_{RA} - 3.49P_{LA} \qquad (3)$$

where V is the stressed blood volume, CO_V is the integrated venous return, and *0.129* (min), *19.61* ($ml \cdot min^{-1} \cdot kg^{-1} \cdot mmHg^{-1}$), *3.49* ($ml \cdot min^{-1} \cdot kg^{-1} \cdot mmHg^{-1}$) are standard parameters characterizing the venous return surface (29). The reference CO, P_{LA} and P_{RA} values were used to calculate V, which served as the reference stressed volume.

With altered V (from +8 to −8 ml·kg^{-1} of the reference value), we numerically determined the intersection of the venous return surface (*Eq. 3*) and the integrated cardiac output curve (*Eq. 1* and *2*) to predict CO, P_{LA} and P_{RA}. The predicted CO, P_{LA} and P_{RA} were compared with those measured. We considered the change in V (± 8 ml·kg^{-1}) as substantial, considering the physiological amount of the stressed blood volume (~25 ml·kg^{-1}) (17).

Statistics

Group data are expressed as means (SD). The level of statistical significance was defined as $p < 0.05$. To test the goodness of fit, the coefficient of determination (r^2) and the standard error of estimate (SEE) were calculated.

RESULTS

Determination of the standard parameters

Figure 3 shows the measured P_{LA}-CO (panel A) and P_{RA}-CO (panel B) relationship in a representative dog. Cardiac output increases in response to increases in either left or right atrial pressure by the Frank-Starling mechanisms. These relationships could be fitted to the 3-parameter logarithmic function (thin solid lines) (Fig. 3A, CO=66.7[ln(P_{LA}-2.08)+0.1], r^2 = 0.98, SEE = 5.9 ml·min^{-1}·kg^{-1}; Fig. 3B, CO=112.7[ln(P_{RA}-1.39)+0.19], r^2 = 0.98, SEE = 5.5 ml·min^{-1}·kg^{-1}).

Table 1 summarizes the results of the fit in 7 dogs. As shown in Tables 1-1 and 1-2, coefficients of determination were high for both the left (r^2=0.95-0.99) and the right heart (r^2=0.90-0.99). These results indicated that the logarithmic functions represented the cardiac

output curves of the left and the right heart with good accuracy. The averaged F and H values (F_L = 2.03 mmHg, H_L = 0.80, F_R = 2.13 mmHg and H_R = 1.90) for 7 animals were used as standard values in subsequent analyses.

Estimation of the integrated cardiac output curve

Figure 4 shows the estimated cardiac output curves under normal (solid lines) and heart failure conditions (dashed lines) of a single animal (Panel A; left heart, Panel B; right heart). Solid circles (normal) and solid squares (heart failure) indicate the reference hemodynamic values. From these reference values, we calculated individual values of the S parameter. Under normal conditions, the estimated cardiac output curve accurately coincided with the measured points (solid lines vs. open circles) in the left and in the right heart. A good agreement was also observed under left ventricular failure (dashed lines vs. open squares).

Figure 5 demonstrates the relationship between estimated and measured cardiac output of pooled data from 7 animals (*Group 1*). The estimated cardiac output agreed with the measured cardiac output in the left heart (Fig. 5A, y = 0.88 x + 13.3, n = 104, r^2 = 0.93, SEE = 8.7 ml·min^{-1}·kg^{-1}), and in the right heart (Fig. 5B, y = 0.96 x + 5.0, n = 104, r^2 = 0.88, SEE = 12.1 ml·min^{-1}·kg^{-1}).

Prediction of circulatory equilibrium

Figure 6 illustrates the accuracy of prediction of hemodynamics in response to changes in stressed blood volume (8 dogs, *Group 2*).

Figure 6A shows the relationship between predicted and measured cardiac output.

Cardiac output was predicted accurately (y=0.93x+6.5, n=128, r^2 = 0.96, SEE = 7.5 ml·min^{-1}·kg^{-1}) over a wide range of cardiac output from 30 to 200 ml·min^{-1}·kg^{-1}. A small intercept value with a nearly unity slope also indicates the accuracy of prediction.

Figure 6B shows the accuracy of the left atrial pressure prediction. Although variability increased in the high pressure range (> 20 mmHg), the prediction was reasonably accurate (y = 0.90 x + 0.5, n = 128, r^2 = 0.93, SEE = 1.4 mmHg).

Likewise, right atrial pressures were also predicted with reasonable accuracy (Figure 6C, y = 0.87 x + 0.4, n = 128, r^2 = 0.91, SEE = 0.4 mmHg).

DISCUSSION

The results of this study indicate that, once a single set of steady-state CO, P_{LA} and P_{RA} values is available, it is possible to predict the changes in hemodynamic variables resulting from a known amount of change in stressed blood volume. This prediction can be very helpful in the management of patients under unstable hemodynamic conditions (13, 23).

Estimation of the integrated cardiac output curve

We have shown that the integrated cardiac output curve can be estimated with reasonable accuracy under normal and heart failure conditions (Figs. 4 and 5). By fixing the F and H parameters and by ascribing the changes in the cardiac output curve exclusively to the S parameter, we were able to estimate the integrated cardiac output curve from a single set of hemodynamic measurements. As shown in Appendix, the F and H parameters are mainly related to end-diastolic pressure-volume relationship (*Eq. A4*). In advanced cardiac disorders seen

clinically, the end-diastolic pressure-volume relationship may vary drastically (6, 7). Hypertensive or idiopathic cardiomyopathy sometimes induces severe ventricular hypertrophy, thereby significantly altering the diastolic ventricular pressure-volume relationship (14). In such cases, it may be desirable not to use fixed values, but to estimate F and H parameters in individual patients. The cardiovascular properties shown in *Eq. A4* can be estimated non-invasively under a steady-state hemodynamic condition (3, 12). Integration of these properties into our method may allow independent estimation of the three parameters in individual patients.

The following validations indicate that our mathematical model of the cardiac output curve and its estimation are consistent with previous investigations. First, based on *Eq. A4* (see Appendix), we calculated the 3 parameters in the logarithmic function for the left heart using previously reported data (6, 11, 18, 25). The values of the cardiovascular properties were chosen to be appropriate for a 20 kg dog (Table 2). The calculated S_L (34 ml·min^{-1}·kg^{-1}), F_L (3.2 mmHg), and H_L (1.14) were compatible with those obtained in our experiment (Table1-1). Second, Pouleur et al. (19) examined the cardiac output curve of the left heart in dogs under various cardiac conditions (control, coronary occlusion, nitroprusside infusion under control and coronary occlusion). Their cardiac output curves could be approximated to our three-parameter logarithmic functions with reasonable accuracy (r^2 = 0.94-0.99). When we applied the standard values of F_L (2.03 mmHg) and H_L (0.80) obtained in this study to their data and estimated their cardiac output curve, the estimated cardiac output closely correlates with the values measured (y = 0.67 x + 29.0, r^2 = 0.90, SEE = 5.0 ml·min^{-1}·kg^{-1}, from 40 to 150 ml·min^{-1}·kg^{-1}).

Clinical application of the framework of circulatory equilibrium

Cardiac patients frequently receive empirical fluid challenges to treat low cardiac output, unexplained hypotension, and oliguria (1, 32). Such empirical challenges sometimes exert deleterious effect by excessive volume expansion (1, 32). Our framework is free of such problems. That is because we can accurately estimate the stressed blood volume of the patient and predict hemodynamics resulting from the volume challenge once we measure a single set of steady-state CO, P_{LA} and P_{RA} values with for example, Swan-Ganz catheters (2).

The outcome of acute or chronic heart failure has been related to the severity of reduced cardiac output and elevated left ventricular filling pressure (4, 5, 13, 23). Several studies, however, indicate that having Forrester class IV hemodynamics does not necessarily condemn patients to a class IV prognosis. Even if the initial hemodynamics are classified as class IV, patients showing reduction in filling pressure following intensive medical therapy have a better prognosis than those without reduction in filling pressure (13, 23). Using our framework for guidance, proper management of low cardiac output and elevated filling pressures would improve the prognosis of such patients.

In clinical settings, the reference point for zero pressure is determined by an empirical external inspection (16). Changes in the patient's position relative to the pressure transducer may induce apparent changes in atrial pressures (16). These factors can result in a measurement error for atrial pressure, and consequently, an error in the prediction of the circulatory equilibrium. Accurate determination of the external reference point relative to the level of the right atrium and paying strict attention to patient position are required for clinical application of our framework.

Limitations of this study

All the experiments of this study were conducted in anesthetized, open-chest dogs.

Anesthesia and surgical trauma significantly affect the cardiovascular system (31). Whether this equilibrium framework can be applied to conscious, closed-chest animals (including humans) remains to be tested.

We isolated baroreceptors and fixed the autonomic tone in this study. This was necessary because the baroreflex alters the cardiac output curve and venous return surface, through its effects on stressed blood volume, vascular resistance, heart rate and cardiac contractility (8, 22). How changes in autonomic tone under the closed loop condition affect the accuracy of hemodynamic prediction remains to be investigated.

Conclusion

The integrated cardiac output curve can be estimated based on a single set of hemodynamic measurements (CO, P_{LA} and P_{RA}). The integrated cardiac output curve thus estimated enables accurate prediction of hemodynamics (CO, P_{LA} and P_{RA}) following extensive changes in stressed blood volume under heart failure conditions as well as during normal cardiac functions.

APPENDIX

Mathematical modeling of the Cardiac Output Curve

We derived the relationship between cardiac output (*CO*) and atrial pressure based on the ventricular pressure-volume relationship framework (15, 25) and the ventricular-arterial coupling framework (26) as follows.

The relationship between the stroke volume (*SV*) and the ventricular end-diastolic volume (V_{ed}) has been approximated with reasonable accuracy as

$$SV = \frac{TE_{es}}{TE_{es} + R} \times (V_{ed} - V_0) \tag{A1}$$

where E_{es} is the slope (elastance) and V_0 is the volume axis intercept of the ventricular end-systolic pressure-volume relationship, T is the heart period and R is the arterial resistance (20, 25, 26). Dividing SV by T, cardiac output (*CO*) can be expressed as

$$CO = \frac{E_{es}}{TE_{es} + R} \times (V_{ed} - V_0) \tag{A2}$$

V_{ed} can be interrelated with end-diastolic pressure (P_{ed}) by:

$$P_{ed} = \alpha e^{kV_{ed}} + \beta \tag{A3}$$

where k, α, and β are constants (6, 7). If we approximate P_{ed} by a scaled mean atrial pressure (P_{At}), γP_{At} (γ is a proportionality constant), *Equation A2* can be rewritten as

$$CO = \frac{1}{k} \cdot \frac{E_{es}}{TE_{es} + R} \times \left[\ln\left(P_{At} - \frac{\beta}{\gamma} \right) + \ln\left(\frac{\gamma}{\alpha} \right) - kV_0 \right] \tag{A4}$$

Equation A4 can be simplified by lumping parameters for cardiovascular system properties into

three constants, S, F, and H.

$$CO = S \times \left[\ln\left(P_{A_l} - F\right) + H\right] \tag{A5}$$

GRANTS

This study was supported by Health and Labor Sciences Research Grants for research on medical devices for analyzing, supporting and substituting the function of the human body and research on advanced medical technology from the Ministry of Health Labour and Welfare of Japan, a Grant-in-Aid for Scientific Research (A 15200040, C 14570707, C 15590786) from the Japan Society for the Promotion of Science, and a Grant-in-Aid for Young Scientists (B)(16700379) from the Ministry of Education, Culture, Sports, Science and Technology, as well as by the Program for Promotion of Fundamental Studies in Health Science of Pharmaceuticals and Medical Devices Agency of Japan.

REFERENCES

1. **Bendjelid K, Suter PM, and Romand JA.** The respiratory change in preejection period: a new method to predict fluid responsiveness. *J Appl Physiol* 96: 337-342, 2004.
2. **Chaliki HP, Hurrell DG, Nishimura RA, Reinke RA, and Appleton CP.** Pulmonary venous pressure: relationship to pulmonary artery, pulmonary wedge, and left atrial pressure in normal, lightly sedated dogs. *Catheter Cardiovasc Interv* 56: 432-438, 2002.
3. **Chen CH, Fetics B, Nevo E, Rochitte CE, Chiou KR, Ding PA, Kawaguchi M, and Kass DA.** Noninvasive single-beat determination of left ventricular end-systolic elastance in humans. *J Am Coll Cardiol* 38: 2028-2034, 2001.
4. **Crexells C, Chatterjee K, Forrester JS, Dikshit K, and Swan HJ.** Optimal level of filling pressure in the left side of the heart in acute myocardial infarction. *N Engl J Med* 289: 1263-1266, 1973.
5. **Forrester JS, Diamond G, Chatterjee K, and Swan HJG.** Medical therapy of acute myocardial infarction by application of hemodynamic subsets (first of two parts). *N Eng J Med* 295: 1356-1362, 1976.
6. **Glantz SA, and Kernoff RS.** Muscle stiffness determined from canine left ventricular pressure-volume curves. *Circ Res* 37: 787-794, 1975.
7. **Glantz SA, and Parmley WW.** Factors which affect the diastolic pressure-volume curve. *Circ Res* 42: 171-180, 1978.
8. **Greene AS, and Shoukas AA.** Changes in canine cardiac function and venous return curves by the carotid baroreflex. *Am J Physiol* 251: H288-H296, 1986.
9. **Guyton AC.** Determination of cardiac output by equating venous return curves with cardiac response curves. *Physiol Rev* 35:123-129, 1955.

10. **Guyton AC, Jones CE, and Coleman TG.** *Circulatory Physiology: Cardiac Output and Its Regulation, 2nd ed.* Philadelphia: WB Saunders, 1973, p. 263-284.

11. **Lee RW, and Goldman S.** Mechanism for decrease in cardiac output with atrial natriuretic peptide in dogs. *Am J Physiol Heart Circ Physiol* 256: H760-H765, 1989.

12. **Little WC, Ohno M, Kitzman DW, Thomas JD, and Cheng CP.** Determination of left ventricular chamber stiffness from the time for deceleration of early left ventricular filling. *Circulation* 92: 1933-1939, 1995.

13. **Lucas C, Johnson W, Hamilton MA, Fonarow GC, Woo MA, Flavell CM, Creaser JA, and Stevenson LW.** Freedom from congestion predicts good survival despite previous class IV symptoms of heart failure. *Am Heart J* 140: 840-847, 2000.

14. **Mandinov L, Eberli FR, Seiler C, and Hess OM.** Diastolic heart failure. *Cardiovasc Res* 45: 813-825, 2000.

15. **Maughan WL, Shoukas AA, Sagawa K, and Weisfeldt ML.** Instantaneous pressure-volume relationship of the canine right ventricle. *Circ Res* 44: 309-315, 1979.

16. **McGee SR.** Physical examination of venous pressure: a critical review. *Am Heart J* 136: 10-18, 1998.

17. **Ogilvie RI, and Zborowska-Sluis D.** Effect of chronic rapid ventricular pacing on total vascular capacitance. *Circulation* 85: 1524-1530, 1992.

18. **Ohno M, Cheng CP, and Little WC.** Mechanism of altered patterns of left ventricular filling during the development of congestive heart failure. *Circulation* 89: 2241-50, 1994.

19. **Pouleur H, Covell JW, and Ross J Jr.** Effects of nitroprusside on venous return and central blood volume in the absence and presence of acute heart failure. *Circulation* 61: 328-337, 1980.

20. **Sagawa K, Maughan WL, Suga H, and Sunagawa K.** *Cardiac Contraction and*

Pressure-Volume Relationship. Oxford, UK: Oxford Univ. Press, 1988, p. 232-298.

21. **Sarnoff SJ, and Berglund E.** Ventricular function. 1. Starling's law of the heart, studied by means of simultaneous right and left ventricular function curves in the dog. *Circulation* 9: 706-718, 1953.
22. **Shoukas AA.** Carotid sinus baroreceptor reflex control and epinephrine. Influence on capacitive and resistive properties of the total pulmonary vascular bed of the dog. *Circ Res* 51: 95-101, 1982.
23. **Stevenson LW, Tillisch JH, Hamilton M, Luu M, Chelimsky-Fallick C, Moriguchi J, Kobashigawa J, and Walden J.** Importance of hemodynamic response to therapy in predicting survival with ejection fraction less than or equal to 20% secondary to ischemic or nonischemic dilated cardiomyopathy. *Am J Cardiol* 66: 1348-1354, 1990.
24. **Stone HL, Bishop VS, and Dong EJ.** Ventricular function in cardiac denervated and cardiac sympathectomized conscious dogs. *Circ Res* 20: 587-593, 1967.
25. **Suga H, and Sagawa K.** Instantaneous pressure-volume relationships and their ratio in the excised, supported canine left ventricle. *Circ Res* 35: 117-126, 1974.
26. **Sunagawa K, Maughan WL, Burkhoff D, and Sagawa K.** Left ventricular interaction with arterial load studied in isolated canine ventricle. *Am J Physiol Heart Circ Physiol* 245: H773-H780, 1983.
27. **Sunagawa K, Sagawa K, and Maughan WL.** Ventricular interaction with the loading system. *Ann Biomed Eng* 12: 163-189, 1984.
28. **Todaka K, Leibowitz D, Homma S, Fisher PE, Derosa C, Stennett R, Packer M, and Burkhoff D.** Characterizing ventricular mechanics and energetics following repeated coronary microembolization. *Am J Physiol Heart Circ Physiol* 272: H186-H194, 1997.
29. **Uemura K, Sugimachi M, Kawada T, Kamiya A, Jin Y, Kashihara K, and Sunagawa K.**

A novel framework of circulatory equilibrium. *Am J Physiol Heart Circ Physiol* 286; H2376-H2385, 2004.

30. **Ursino M.** Interaction between carotid baroregulation and the pulsating heart: a mathematical model. *Am J Physiol* 275: H1733-H1747, 1998.

31. **Vatner SF, and Braunwald E.** Cardiovascular control mechanisms in the conscious state. *N Engl J Med* 293: 970-976, 1975.

32. **Wagner JG, and Leatherman JW.** Right ventricular end-diastolic volume as a predictor of the hemodynamic response to a fluid challenge. *Chest* 113: 1048-1054, 1998.

LEGENDS

Fig. 1. Diagram of circulatory equilibrium for cardiac output (CO), venous return (CO_V), left atrial pressure (P_{LA}), and right atrial pressure (P_{RA}). The equilibrium CO, P_{LA} and P_{RA} are obtained as the intersection point of the venous return surface and the integrated cardiac output curve [modified from Uemura et al. (Ref. 29)].

Fig. 2. Changes in arterial pressure, CO, P_{LA} and P_{RA} throughout the examination. As P_{RA} and P_{LA} decreases following stepwise reduction of the stressed blood volume, CO also decreases (Frank-Starling mechanism).

Fig. 3. The relationship between CO and P_{LA} (A), and between CO and P_{RA} (B) in a single dog. Thin solid lines represent the best fit curves of the 3-parameter logarithmic functions obtained by the least square method.

Fig. 4. Cardiac output curves for a single animal under normal and left ventricular failure conditions for the left heart (A) and the right heart (B). •, reference hemodynamic values under normal conditions; ■, reference hemodynamic values under left ventricular failure; ○, measured points under normal conditions; □, measured points under left ventricular failure conditions. Estimated cardiac output curves under normal conditions (solid lines) and under left ventricular failure conditions (dashed lines) accurately correspond with the measured points.

Fig. 5. Relationship between estimated and measured values of CO for the left heart (A), and the right heart (B) for 104 steps pooled over 13 output curves. •, normal cardiac function; ○, left

heart failure; dashed line, lines of identity. Regression analysis (solid line) reveals that estimated *CO* agrees well with measured *CO* in the left heart (y = 0.88 x + 13.3, n = 104, r^2 = 0.93, SEE = 8.7 ml·min^{-1}·kg^{-1}), and right heart (y = 0.96 x + 5.0, n = 104, r^2 = 0.88, SEE = 12.1 ml·min^{-1}·kg^{-1}).

Fig. 6. Relationship between predicted and measured values for *CO* (*A*), P_{LA} (*B*) and P_{RA} (*C*) for 128 steps. •, normal cardiac function; ○, left heart failure; dashed line, lines of identity. Prediction was done by intersecting the venous return surface and the integrated cardiac output curve, both of which were estimated from a set of reference hemodynamic values. Regression analysis (solid line) reveals that predicted *CO* (y=0.93x+6.5, n=128, r^2 = 0.96, SEE = 7.5 ml·min^{-1}·kg^{-1}), P_{LA} (y = 0.90 x + 0.5, n = 128, r^2 = 0.93, SEE = 1.4 mmHg), and P_{RA} (y = 0.87 x + 0.4, n = 128, r^2 = 0.91, SEE = 0.4 mmHg) agree reasonably well with measured values.

Table 1-1. *Summary of the fit of the relationship between cardiac output and left atrial pressure to 3-parameter logarithmic functions*

Dog No.	S_L	F_L	H_L	r^2	SEE
1	58.1	1.27	0.61	0.98	4.3
2	24.4	2.03	2.71	0.95	3.6
3	108.4	0.00	-0.67	0.95	5.6
4	66.7	2.08	0.08	0.98	5.9
5	105.6	2.30	-0.02	0.99	5.0
6	73.5	2.21	0.59	0.99	2.5
7	42.0	4.32	2.30	0.98	4.7
MEAN (SD)	68.4 (30.9)	2.03 (1.29)	0.80 (1.25)	0.97	4.5 (1.2)

S_L ($ml \cdot min^{-1} \cdot kg^{-1}$), F_L (mmHg) and H_L (unitless) are the parameters of the logarithmic function for the left heart. See **METHODS** for calculations. r^2, coefficient of determination. SEE, standard error of the estimate ($ml \cdot min^{-1} \cdot kg^{-1}$).

Table 1-2. *Summary of the fit of the relationship between cardiac output and right atrial pressure to 3-parameter logarithmic functions*

Dog No.	S_R	F_R	H_R	r^2	SEE
1	46.7	2.12	2.34	0.98	4.7
2	33.9	1.50	2.50	0.96	3.3
3	64.1	2.10	2.10	0.90	8.2
4	112.7	1.39	0.19	0.98	5.5
5	101.8	1.39	0.92	0.99	4.6
6	80.6	3.07	1.59	0.99	2.8
7	37.1	3.33	3.69	0.94	6.8
MEAN (SD)	68.1 (31.3)	2.13 (0.8)	1.90 (1.14)	0.96	5.1 (1.9)

S_R ($ml \cdot min^{-1} \cdot kg^{-1}$), F_R (mmHg) and H_R (unitless) are the parameters of the logarithmic function for the right heart. See **METHODS** for calculations. r^2, coefficient of determination. SEE, standard error of the estimate ($ml \cdot min^{-1} \cdot kg^{-1}$).

Table 2. *Values of the cardiovascular properties from previously reported data*

HR, beats/min	120
T, min	0.0083
R, mmHg·min·ml^{-1}	0.031
E_{es}, mmHg·ml^{-1}	10
V_0, ml	5
k, ml^{-1}	0.13
α, mmHg	0.25
β, mmHg	4.8
γ (unitless)	1.5

HR, heart rate; *T*, heart period; *R*, systemic arterial resistance ; E_{es}, end-systolic elastance of left ventricle; V_0, volume at which end-systolic pressure is 0 mmHg in left ventricle; *k*, α, and β, constants characterizing the end-diastolic pressure-volume relationship of the left ventricle; γ, ratio of left ventricular end-diastolic pressure to mean left atrial pressure. See Appendix for abbreviations.

Figure1

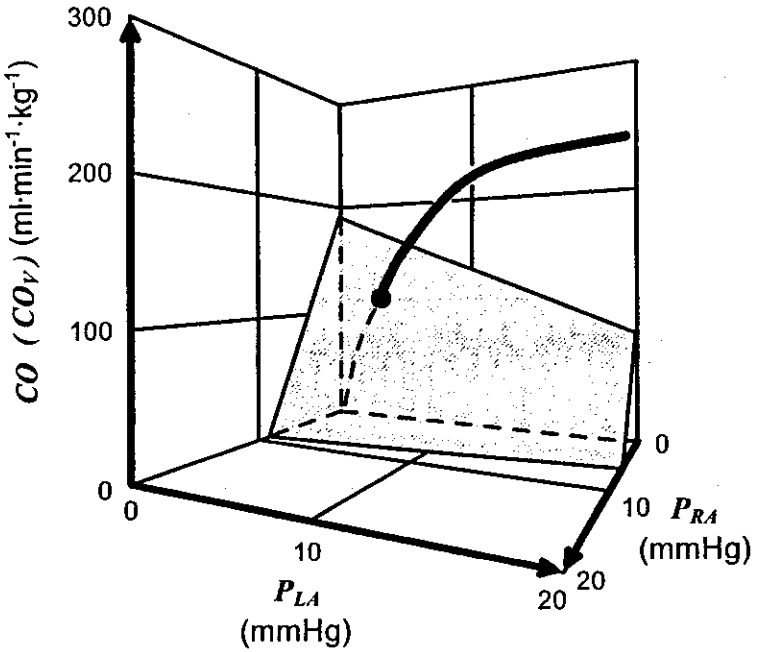

Figure 2

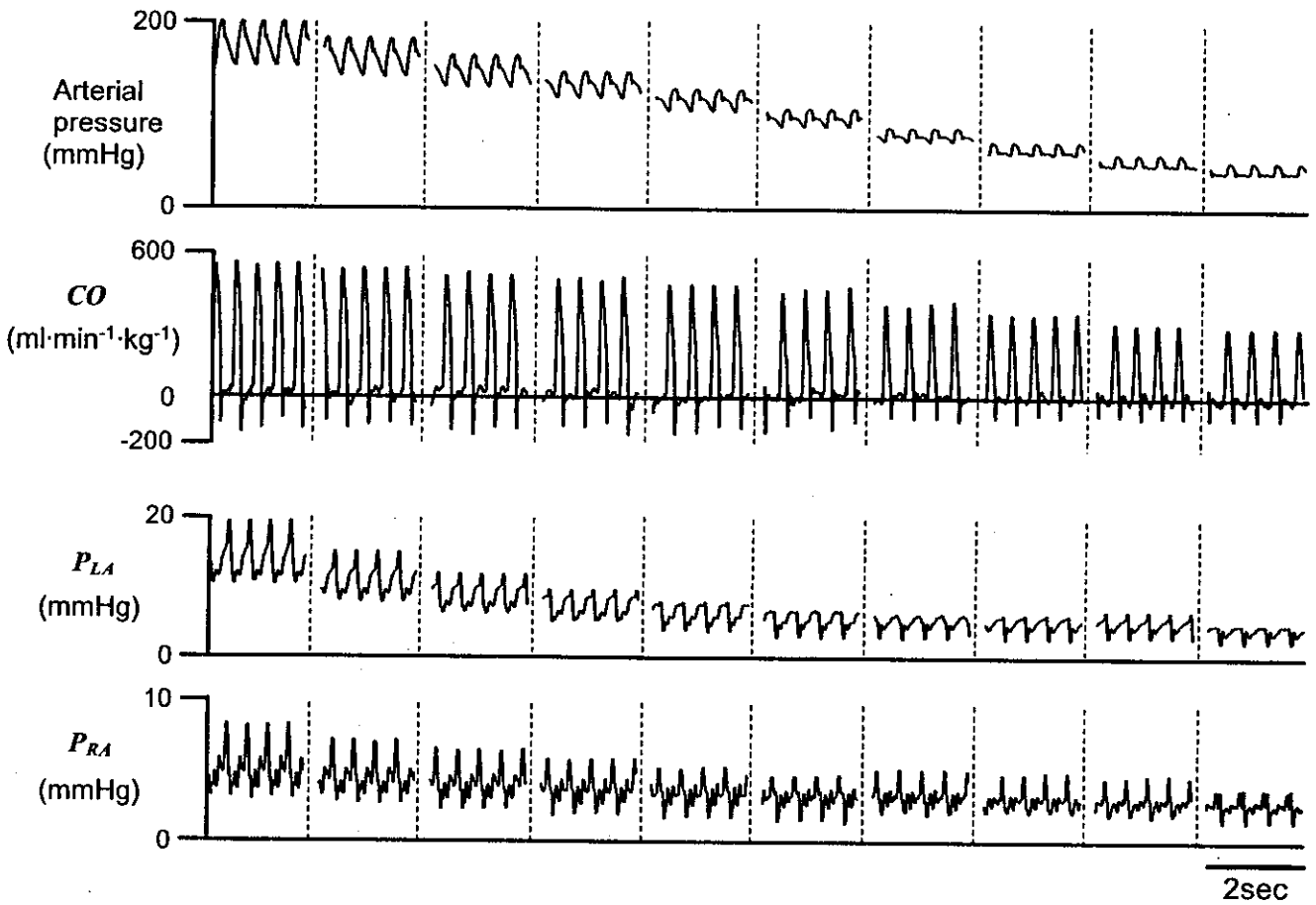
200
Arterial pressure (mmHg)
0
600
CO
(ml·min-1·kg-1)
0
-200
20
PLA
(mmHg)
0
10
PRA
(mmHg)
0
2sec